



Published in final edited form as:

Nanoscale. 2017 September 21; 9(36): 13465–13476. doi:10.1039/c7nr02363d.

NIR-emissive PEG-*b*-TCL Micelles for Breast Tumor Imaging and Minimally Invasive Pharmacokinetic Analysis

Christina L. Hofmann^a, Melanie C. O'Sullivan^b, Alexandre Detappe^{c,d,e}, Yingjie Yu^c, Xi Yang^c, Wei Qi^b, Chelsea D. Landon^f, Michael J. Therien^b, Mark W. Dewhirst^{a,f,g}, P. Peter Ghoroghchian^{c,d,e,*}, and Gregory M. Palmer^{g,*}

^aBiomedical Engineering Department, Duke University, Room 136 Hudson Hall, Durham, NC 27708, USA

^bDepartment of Chemistry, Duke University, French Family Science Center, 124 Science Drive, Durham, NC 27708, USA

^cDana-Farber Cancer Institute, 450 Brookline Avenue, Boston MA, 02215, USA

^dHarvard Medical School, 25 Shattuck St, Boston, MA 02115

^eKoch Institute for Integrative Cancer Research at Massachusetts Institute of Technology, 77 Massachusetts Avenue, Room 76-261F, Cambridge MA, 02139, USA

^fDepartment of Pathology, Duke University Medical Center, Box 3455, Durham, NC 27710, USA

^gRadiation Oncology Department, Duke University Medical Center, Box 3455, Durham, NC 27710, USA

Abstract

Motivated by the goal of developing a fully biodegradable optical contrast agent with translational clinical potential, a nanoparticle delivery vehicle was generated from the self-assembly of poly(ethylene-glycol)-block-poly(trimethylene carbonate-co-caprolactone) (PEG-*b*-TCL) copolymers. Cryogenic transmission electron microscopy verified that PEG-*b*-TCL-based micelles were formed at low solution temperatures (~ 38 °C). Detailed spectroscopic experiments validated facile loading of large quantities of the high emission dipole strength, tris(porphyrin)-based fluorophore PZn₃ within their cores, and the micelles displayed negligible *in vitro* and *in vivo* toxicities in model systems. The pharmacokinetics and biodistribution of PZn₃-loaded PEG-*b*-TCL-based micelles injected intravenously were determined via *ex vivo* near-infrared (NIR) imaging of PZn₃ emission in microcapillary tubes containing minute quantities of blood, to establish a novel method for minimally invasive pharmacokinetic monitoring. The *in vivo* circulatory half-life of the PEG-*b*-TCL-based micelles was found to be ~19.6 h. Additionally, longitudinal *in vivo* imaging of orthotopically transplanted breast tumors enabled determination of micelle biodistribution that correlated to *ex vivo* imaging results, demonstrating accumulation

*Co-senior authors and to whom correspondence should be addressed: P. Peter Ghoroghchian, MD, PhD, Koch Institute for Integrative Cancer Research, 77 Massachusetts Avenue, 76-261F, Boston, MA 02139, Tel: +1 (617) 715-4470, ppg@mit.edu. Greg Palmer, Ph.D., Radiation Oncology Department, Duke University Medical Center, Box 3455, Durham, NC 27710, USA, Tel: +1 (919) 613-5053, Fax: +1 (919) 684-8718, greg.palmer@duke.edu.

CONFLICTS OF INTEREST

There are no conflicts to declare.

predominantly within the tumors and livers of mice. The PEG-*b*-TCL-based micelles quickly extravasated within 4T1 orthotopic mammary carcinomas, exhibiting peak accumulation at ~48 h following intravenous tail-vein injection. In summary, PEG-*b*-TCL-based micelles demonstrated favorable characteristics for further development as *in vivo* optical contrast agents for minimally invasive imaging of breast tumors.

Keywords

biodistribution; micelle; nanoparticle; near infrared; optical imaging; pharmacokinetics; tumor imaging

INTRODUCTION

Over the past several decades, significant progress has been made in the construction of target-specific and near-infrared (NIR) emissive optical probes (1, 2). For *in vivo* imaging, the magnitude of any fluorescent signal is mainly dictated by its emission wavelength, its fluorescent quantum yield, the amount of fluorophore that may be delivered to a specific site, the tissue type, and the depth of imaging (3). For instance, Lumicell is one of a few NIR emitters that have been developed for intraoperative imaging of lymph nodes during breast surgery, which is a highly invasive but potentially paradigm-shifting technique that may prolong the lives of breast cancer patients (4). NIR imaging may find broader utility in less invasive diagnostic applications, however the lack of a safe, biodegradable, and organic-based contrast agent with the requisite optical characteristics has hitherto been a major technical hurdle to realizing the full potential of deep-tissue and fluorescence-based imaging (3, 5–7).

Here, we sought to generate self-assembled and biodegradable nanoparticles comprised of poly(ethylene glycol)-*block*-poly(trimethylene carbonate-*co*-caprolactone) copolymers (PEG-*b*-TCL) for delivery of an organic-based optical imaging agent to solid tumors (Scheme 1A). Our previous work has helped to establish the nanoscale morphologies adopted by PEG-*block*-(ϵ -caprolactone)- (PEG-*b*-PCL)-based diblock copolymers upon aqueous dispersion (8, 9). In order to generate a robust yield of fluid-phase micelles that could be formed at lower temperatures (i.e. < 60 °C) and without the need of an organic cosolvent system that could introduce additional processing steps and/or toxicities for *in vivo* applications, we sought to study the nanoscale architectures derived from aqueous dispersion of PEG-*b*-TCL polymers. PEG-*b*-TCL-based nanoparticles were expected to possess fully PEGylated surfaces that could prolong *in vivo* circulation times and afford tumor accumulation via the EPR effect (10, 11). The degradation products of TCL would also be expected to be non-acidic, in contrast to the monomeric byproducts of other commonly utilized aliphatic polyesters (3, 9), which would provide improved control over degradation kinetics and formulation stability (12).

To generate fully biodegradable and organic-based contrast agents for translational clinical imaging applications, we focused on utilizing the tris(porphyrin)-based NIR-fluorophore PZn₃ as the emissive component of our system (Scheme 1A). This high emission dipole strength, supermolecular fluorophore is known to possess exceptionally large vis-NIR molar

absorptive oscillator strength, to display amongst the highest recorded fluorescence emission quantum yields in the NIR spectral region, and to exhibit an enhanced photobleaching threshold (3, 13, 14). It was expected that PZn₃-loaded PEG-*b*-TCL-based micelles would offer the following advantages over other contrast agents that have previously been developed for *in vivo* optical imaging: (i) a high yield of fluorophore-laden micelles could be generated under gentle fabrication conditions (Scheme 1B); (ii) modest PZn₃ loading would correspond to dispersion of thousands of fluorophores in a single delivery vehicle (7, 15); and, (iii) as the components of this soft matter assembly are derived from natural and biodegradable components (i.e., porphyrins and poly(esters)) (3, 7, 9, 15–21), PZn₃-loaded PEG-*b*-TCL-based micelles would be expected to be a safe contrast agent with the requisite properties for translational *in vivo* imaging applications.

In the studies described herein, we examined both the *in vitro* and *in vivo* toxicities of this novel biodegradable system and utilized NIR optical imaging to study its *in vivo* pharmacokinetics (PK) and tumor accumulation (Scheme 1C). A common limitation encountered in many preclinical PK studies is the necessity to sacrifice a multitude of animals at different time points in order to collect both organs and blood samples for nanoparticle and drug analyses (22–25). We have previously shown that whole-body NIR-based optical imaging is an inexpensive and easy to use imaging modality that enables noninvasive *in vivo* biodistribution studies to be conducted in mice (3, 17). Here, we introduce a novel method to study the PK of PEG-*b*-TCL-based micelles, utilizing *ex vivo* optical imaging of microcapillary tubes containing minute blood samples collected from the same mouse and over several days, which is a minimally invasive technique that eliminates the need for animal sacrifice. Finally, we examine the potential of PEG-*b*-TCL-based micelles for tumor delivery, utilizing NIR optical imaging to validate tumor accumulation in an orthotopically-implanted mammary carcinoma model.

MATERIALS AND METHODS

Synthesis of PEG-*b*-TCL diblock copolymers

A reaction scheme for the generation of PEG-*b*-TCL is depicted in Supplemental Scheme S1. ϵ -Caprolactone (CL, 1.9 g, Aldrich) was dried over calcium hydride (CaH₂) at room temperature for 48 h and distilled under reduced pressure. Monomethoxy-poly(ethylene glycol) (mPEG, 2kDa, Fluka), featuring a terminal -OH group, was purified by dissolution in tetrahydrofuran (THF), followed by precipitation into diethyl ether and subsequent drying at 40 °C under reduced pressure (10 mm Hg) for 24 h. Polymer grade 1, 3-trimethylene carbonate (TMC, Boehringer Ingelheim), stannous octoate (SnOct₂, stannous 2-ethylhexanoate, Sigma), and 1,6-hexanediol (Aldrich) were used as received.

PEG-*b*-TCL was synthesized by ring-opening polymerization (8, 9). In brief, mPEG was delivered to a flamed-dried flask under argon. A known mass of each CL (5.7 mL) and TMC monomer (2.25 g) were injected into the flask via a syringe. Two drops of SnOct₂ were then added to the reaction mixture; the flask was evacuated and immersed in an oil bath at 130 °C; and, a progressive increase in viscosity of the homogeneous mixture was evident as the polymerization reaction progressed. After 24 h, the volatiles were removed; the recovered solid residue was dissolved in methylene chloride (DCM); and, the polymer was

precipitated with cold methanol/hexane (4 °C). The resulting PEG-*b*-TCL copolymers were dried under vacuum before size fractionation by HPLC and their subsequent characterization by GPC and ¹H-NMR spectroscopy in CDCl₃.

Synthesis of Tris(Porphyrin-based) NIR-Emissive Fluorophore PZn₃

The *meso-to-meso* ethynyl-bridged tris[(porphinato)zinc]-based fluorophore (5,15-bis[[5',-10',20'-bis[3,5-di(3,3-dimethyl-1-butylloxy)phenyl]porphinato)zinc(II)]ethynyl]-10,20-bis[3,5-di(9-methoxy-1,4,7-trioxanonyl)phenyl]porphinato)zinc(II) (PZn₃) was synthesized as previously described (26). In brief, (5,15-dibromo-10,20-bis[3,5-bis(9-methoxy-1,4,7-trioxanonyl)phenyl]porphinato)zinc(II) 5 (0.692 g, 5.19 × 10⁻⁴ mol), Pd(PPh₃)₄ (0.046 g, 3.98 × 10⁻⁵ mol), and CuI (0.023 g, 1.21 × 10⁻⁴ mol) were added to a 100 mL Schlenk tube. Following the addition of 40 ml of dry THF, a solution of (5-ethynyl-10,20-bis[3',5'-bis(3,3-dimethyl-1-butylloxy)phenyl]porphinato)zinc(II) (0.307 g, 3.23 × 10⁻⁴ mol) and diethylamine (0.60 ml, 5.80 × 10⁻³ mol) in 30 ml of dry THF was added via canula. The reaction mixture was stirred under N₂ at 55 °C for 65 h, after which time it was quenched with water. The organic layer was extracted with CHCl₃, washed with water, dried over CaCl₂, and evaporated. The residue was chromatographed on silica gel using 1:1 hexanes:THF as the eluent. Analytical data for the PZn₃ chromophore matched those reported previously; syntheses of key precursor molecules are described in this publication (26).

Micelle Formation

Cryogenic transmission electron microscopy (cryo-TEM) was utilized to select for specific PEG-*b*-TCL compositions that self-assembled into micelles in dilute suspension upon aqueous hydration of the polymer and addition of heat/sonication at 40 °C as previously described (7). Briefly, aqueous suspensions of different molecular weight fractions of the PEG-*b*-TCL diblock copolymer were suspended in solution (~2 μL), deposited onto Quantifoil R2/1 holey carbon TEM grids (Electron Microscopy Sciences, Q225-CR1), and blotted to create a thin film within the humidity-controlled environment of an FEI Mark III Vitrobot. The samples were then vitrified by plunging them into liquid ethane. The grids were stored in liquid nitrogen before being transferred to the Gatan cryogenic holder. The samples were then imaged on a TEM instrument (FEI Tecnai G² TWIN, 200kV). Dynamic light scattering (DLS) (Malvern Zetasizer, Malvern Instruments) was used to measure the hydrodynamic radius of the resultant particles. Samples were measured for 10 s per run; the Malvern software optimized the number of runs per experiment; and the experiments were carried out in triplicate. The histogram results were then averaged and the data are presented as percent intensity versus hydrodynamic radius.

Loading of PZn₃ within PEG-*b*-TCL-based micelles

PEG(2k)-*b*-TCL(11.2k) diblock copolymer was found to generate micelles of 60 nm in diameter by cryo-TEM, corresponding to 110 nm by DLS. To generate NIR-emissive micelle constructs, the polymer was dissolved along with PZn₃ in DCM at a molar ratio of 40:1. The polymer/PZn₃ solution was then placed on roughened Teflon® and dried under vacuum overnight. Each polymer/PZn₃ film was hydrated with phosphate buffered saline

(PBS, pH 7.4, 290 mOsm/kg) at 40 °C for 1 h. Following hydration, the films were sonicated at 40 °C for approximately 90 min. The micelles were then subjected to 10 freeze/thaw cycles by submerging in liquid nitrogen followed by sonication at 40 °C, forming a distribution of nano-sized micelles centered at around 110 nm in diameter as measured by DLS. The zeta potential of the particles was also examined and found to be slightly negative to neutral, which was consistent with the results previously obtained with other PEGylated nanoparticles with and without PZn₃ (15, 16). The monodisperse micelle suspensions were sterilized by filtration through a 0.45 µm syringe filter, concentrated to 5 mg/mL using Millipore Amicon® Ultra centrifugal filter units (10k MWCO), and stored as aliquots at -20 °C.

For determination of PZn₃ concentrations and emission intensities, aqueous suspensions (in PBS) of PZn₃-loaded PEG-*b*-TCL-based micelles were placed in 2 or 10 mm quartz optical cells and electronic absorbance spectra were collected for membrane-incorporated PZn₃ using a Shimadzu spectrophotometer. The extinction coefficients of the PZn₃-loaded micelles at 497 and 777 nm were determined from known concentrations in PBS using Beer's Law. Using the absorbance spectra of PZn₃-loaded PEG-*b*-TCL-based micelles and the calculated extinction coefficients, the micelle concentrations (mg/mL) in unknown samples could be determined (based on the initial 40:1 loading ratio of PEG-*b*-TCL to PZn₃), following established methodologies (15, 16). At these molar ratios, approximately 100% of the PZn₃ fluorophore was expected to have been loaded within the nanoparticles (15, 16). A correction factor was applied to remove scatter. Fluorescence spectra were measured on an Edinburgh FLSP920 equipped with a Hamamatsu R2658 PMT; a Xe900 xenon arc lamp was utilized as the excitation source. All spectra were corrected for spectral throughput and detector sensitivity based on calibrations from a NIST calibrated light source provided by Edinburgh Instruments.

***In vitro* Toxicity Studies**

Human umbilical vein endothelial cells (HUVEC, Lonza CC-2517) were cultured in EGM-2 (Lonza; +1% antibiotic/antimycotic). 4T1 mammary carcinoma cells (ATCC®, CRL-2539) were cultured in DMEM (Gibco®; +1% antibiotic/antimycotic and +10% fetal bovine serum, Sigma). Human mammary epithelial cells (HMEC, Lonza CC-2551) were cultured in MEGM (Lonza; +0.5% antibiotic/antimycotic, Sigma). All cells were maintained at 37 °C with 5% CO₂.

The CellTiterGlo luminescent cellular viability assay (for HUVECs) and a modified clonogenic assay (for HMEC and 4T1 cells) were used to study the *in vitro* toxicities of the PZn₃-loaded micelles. For the CellTiterGlo assay, HUVECs were plated at 2×10³ cells/well and were allowed to reach 80–90% confluence. The cells were subsequently treated with 0, 25, 125, 250, or 450 µg/mL of a suspensions of the 60 nm-diameter (by cryo-TEM) PEG-*b*-TCL-based micelles or with cisplatin (20 µg/mL; positive control) in media with 10% Dulbecco's PBS (DPBS, Gibco®). 72 h after addition of each treatment group, cellular viability was assessed by luminescence and compared to that of cells that received media alone. For the clonogenics assay, HMECs and 4T1 cells were plated in 12-well plates (1×10⁵ HMECs or 2×10⁴ 4T1 cells/well), allowed to attach overnight, and treated with the same

experimental groups when they reached 50–70% confluency. At 24 h after treatment, the cells were rinsed with DPBS and were trypsinized. Trypsinized cells were collected, along with the cells in the initial media and the DPBS rinse for each treatment, and then pelleted by centrifugation. All cells were resuspended in media, counted, plated in 6-well plates at lower density (1000 HMEC cells/well and 750 4T1 cells/well), and allowed to grow for an additional 4–10 days. Colonies were defined as containing at least 20 cells for HMECs and 50 cells for 4T1s.

Cells were fixed (10% methanol and 10% acetic acid), stained (2% crystal violet in 20% ethanol for HMECS and 0.4% crystal violet for 4T1s), and then counted by hand or with a ColCount instrument (Oxford Optronix). The resulting colony numbers were normalized to the plating efficiency of each cell line (DPBS control). Clonogenic assays were repeated for a total of 3 experimental runs that each contained 5–6 measurements per sample point. Results are reported as average surviving fraction \pm standard error. One-way ANOVA was carried out to determine micelle- and dose-dependent toxicity in each cell line. An unpaired 2-sided t-test was then used to determine significance between each treatment and the PBS control.

***In vivo* Toxicity Studies**

Animal studies were conducted under a protocol approved by the Duke University Institutional Animal Care and Use Committee. Female BALB/c mice were used for all *in vivo* studies. Tail veins were catheterized using 30G needles and heparinized saline. PBS (control), unloaded, or PZn₃-loaded PEG-*b*-TCL-based micelles (150 μ L of 5 mg/mL polymer in PBS; 2.5 mol% PZn₃; $\lambda_{em}(max) = 804$ nm) were introduced via IV tail-vein injection (n=6 animals per group). Mice were monitored for signs of toxicity (i.e., lethargy, absence of grooming, weight loss) and by daily weights. At 3 and 14 days post-treatment, 3 mice from each group were randomly selected for sacrifice. Immediately prior to euthanasia, terminal blood draws were conducted via cardiac puncture for serology studies and blood count enumeration. After sacrifice, organs were harvested and fixed with formalin for H&E analysis.

***In vivo* Optical Imaging**

All NIR imaging was conducted using an IVIS[®] Kinetic Imaging Instrument equipped with a Xenogen XGI-8 Gas Anesthesia system (Perkin Elmer, $\lambda_{ex} = 745$ nm, $\lambda_{em} = 810$ –875 nm). Fluorescence images were analyzed with the Living Image[®] 4.2 software by measuring radiant efficiency of regions of interest (ROIs). Radiant efficiency ([photons/s]/[μ W/cm²]) was used to correct for non-uniform excitation and differences in exposure times, providing a consistent measurement between samples (27).

Novel Optical Methods for Minimally Invasive Pharmacokinetic Analysis

Female BALB/c mice were shaved and any residual hair was removed by topical treatment with Nair[®]. Mice received subcutaneous saline at 1.5 h after treatment to avoid dehydration (5 mL/kg). Blood was collected at 1, 2.5, 4, 6, and 24 h post administration of the PZn₃-loaded PEG-*b*-TCL-based micelle suspension. Using a 5.5 mm lancet (Goldenrod), blood was drawn from the submandibular vein and collected directly into heparinized capillary

tubes (Kimble; 15–100 μL). The capillary tubes were centrifuged for 3 min and were immediately imaged after placement on the imaging bed of the IVIS[®] Kinetic instrument. The total radiant efficiency of the plasma in each capillary tube was measured in a ROI of consistent dimensions.

The standard curve for radiant efficiency versus micelle concentration was first determined by adding solutions of known concentrations of PZn₃-loaded PEG-*b*-TCL-based micelles to untreated plasma and by measuring fluorescence from the capillary tubes. Micelle concentrations in plasma samples were then calculated based on this standard curve. PK results were plotted as a function of plasma micelle concentration versus time and were corrected for the decay in PZn₃-emission in plasma tubes, which occurred at an average half-life over three runs of ~58 h. Note that the decay lifetime was significantly longer than the raw *in vivo* plasma half-life of the micelle fluorescence (15.5 h), indicating the plasma fluorescence is decreasing primarily due to clearance *in vivo*. The area under the curve for 0–24 hours (AUC), plasma half-life, and mean residence time (MRT) were computed using the PK library in R via the non-compartmental estimation function (NCA).

***In vivo* Biodistribution Experiments in Non-tumor Bearing Mice**

The female BALB/c mice that were used in the PK study were simultaneously utilized for biodistribution analysis using whole-animal NIR-based optical imaging. Mice were imaged after treatment with 1.5–3% isoflurane at 2 L/min via nosecone, using the IVIS[®] Kinetic Instrument. Each imaging session lasted less than 20 min. At 24 h, the mice were sacrificed by intraperitoneal (IP) injection of Euthazol[®] (50 μL), and their major tissues were collected for *ex vivo* fluorescence imaging. The tissues (bladder, bone, brain, cecum, colon, eye, fat, heart, kidneys, liver, lungs, ovary and duct, small intestine, spleen, and stomach) were placed directly on the imaging bed of the IVIS[®] Kinetic Instrument. ROIs were drawn around each organ to quantify average radiant efficiency. An untreated mouse was used as a control for these biodistribution studies. The ratios of spleen/liver radiant efficiencies for each treatment were analyzed using an unpaired, 2-sided t-test.

Tumor Accumulation

4T1 mouse mammary carcinoma cells that constitutively expressed RFP and that exhibited hypoxia-inducible factor 1 (HIF-1)-coupled GFP emission were cultured in DMEM supplemented with 10% FBS and 1% antibiotic/antimycotic (28). Cells were trypsinized and rinsed 3 times with PBS and then resuspended in serum-free DMEM. The 4T1 cells (100 μL of 5.5×10^6 cells/mL suspension) were injected into the mammary fat pad of female BALB/c mice to generate the orthotopic model of breast cancer.

The tumors were allowed to reach 5 mm in diameter, which took approximately 5–7 days after transplantation; and, the mice were then administered PZn₃-loaded PEG-*b*-TCL-based micelles via IV tail-vein injection (n = 4 animals). The mice were subsequently imaged in an analogous fashion to that which was described in the biodistribution study. Optical imaging was conducted at 0, 3.5, 6.5, 12, 24, 48, and 72 h after micelle administration. A ROI was drawn around the tumor at each time point; each mouse was imaged in three different orientations, and the average tumor radiant efficiency was plotted versus time. Mice were

monitored for weight loss, tumor size, and mobility after micelle injection and were sacrificed when weight loss exceeded 15% of their initial body weight, their tumors inhibited their mobility, or at the termination of the imaging study, which concluded at 72 h after micelle injection. Following sacrifice, the organs and tumors were harvested and *ex vivo* imaging was conducted as previously described. An unpaired, 2-sided t-test was used to compare the *ex vivo* tumor radiant efficiencies.

RESULTS

Micelle Characterization and Loading of PZn₃

Using HPLC-based separation, various molecular weight fractions of PEG-*b*-TCL were first isolated after synthesis of the block copolymer by ring opening polymerization. Cryogenic transmission electron microscopy (cryo-TEM) was utilized to screen for specific PEG-*b*-TCL compositions that self-assembled into micelles in dilute aqueous suspension, following hydration of the dry polymer and the addition of heat/sonication. The molecular weight fraction of the PEG-*b*-TCL that generated a mono-dispersed suspension of polymeric micelles was determined by GPC-MALS (Figure S1A). ¹H-NMR spectroscopy in CDCl₃ confirmed that this formulation consisted of PEG (2kDa)-*b*-TCL (11.2kDa) and revealed that the copolymer structure consisted of a ratio of PEG:CL:TMC of 45:72:26 in the final product (Figure S1B). Differential scanning calorimetry (DSC) confirmed that the copolymer had melting temperatures (T_m s) of 8.8, 21.6, and 38.2 °C (Figure 1); from this DSC data on the neat polymer, one can infer that a fluid-like phase is likely to occur within PEG-*b*-TCL-based micelles upon spontaneous self-assembly at an aqueous temperature of > 38 °C.

PZn₃ was loaded within the hydrophobic core of the micelles following previously established methodologies (7, 14, 15); and, cryo-TEM confirmed that stability of the micelle architecture when loaded with PZn₃ at ~2.5 mol% (Figure 2A), which is a loading level that has been previously been shown in multiple polymeric vehicles to maximize emission on a per particle basis (15, 16). Aqueous absorption and emission spectra demonstrated the characteristic peaks of this water-insoluble NIR-emissive fluorophore when present within the hydrophobic core of the micelles; the spectral signatures were nearly identical to those observed for PZn₃ in organic solution (Figure 2B); and, given our previous experiences with the development of polymeric delivery vehicles for this fluorophore (3, 7, 8, 14, 17, 18), the emission of PZn₃-loaded PEG-*b*-TCL-based micelles was of requisite intensity to enable *in vivo* optical imaging.

Structural and Optical Stability of PZn₃-loaded PEG-*b*-TCL-based Micelles

In preparation for subsequent *in vitro* and *in vivo* experimentation, we next sought to investigate the emissive and structural stability of PZn₃-loaded PEG-*b*-TCL-based micelles in different *in situ* environments. A concentrated solution of micelles was formed in PBS buffer at pH 7.4 and aliquots were transferred into larger volume solutions of either neutral (PBS, pH 7.4) or acidic pH (sodium acetate buffer, pH 5.5). DLS measurements verified the stability of the hydrodynamic diameter of the micelles in either suspension and as measured

over a 30-day period, establishing that the micelles did not substantially aggregate in either pH environment (Figure 2C).

The intensity of the PZn₃ emission from PEG-*b*-TCL-based micelles slowly diminished as a function of time (Figure 2D). Measurements of kinetic changes in the AUC helped to determine that the half-life of PZn₃ emission in the micelle environment was ~58 h (Figure 2D), and the diminished intensities were likely attributable to release of PZn₃ from the micelles followed by subsequent fluorescence quenching in the aqueous environment (15, 16). Additional experimental runs yielded consistent results (Figure S2). Notably, as the half-life of PZn₃ emission was substantially longer than the expected half-life of circulation for the PEG-*b*-TCL-based micelles, which was likely to be < 24 h based on their PEGylated surfaces and their nanoscaled size distributions (29), additional experiments aimed at examining the *in vitro* and *in vivo* performance were carried out.

***In vitro* and *In vivo* Toxicity Studies**

For successful translational applications, it was imperative to screen for potential toxicities of our proposed optical contrast agent (3). As *in vitro* model systems, we utilized several established cell lines as well as different cellular viability assays. As the PZn₃-loaded PEG-*b*-TCL-based micelles were expected to have prolonged circulation times, their potential vascular toxicities were examined using human umbilical vein endothelial cells (HUVECs) by adopting the CellTiterGlo luminescence assay. Additional toxicities for the same formulation were studied using human mammary epithelial cells (HMECs) and 4T1 mammary carcinoma and by adopting a clonogenic assay; these later cell lines were selected in order to examine differential toxicities that could be imparted by PZn₃-loaded PEG-*b*-TCL-based micelles to normal vs. cancerous cells after *in vivo* extravasation within tumor sites.

In all cases, the cells were incubated with the micelles for 72 h and various concentrations were examined, ranging from 25–450 µg/mL. This range was selected in order to simulate the tissue exposure levels that would typically be seen during *in vivo* optical imaging applications. For example, intravascular (IV) tail-vein injection of 150 µL of a 5 mg/mL suspension of PZn₃-loaded polymeric vesicles has previously been shown to enable deep-tissue optical imaging (3, 8, 17, 20); this dose correlates to a maximum blood concentration of 325 µg/mL immediately after injection. PZn₃-loaded PEG-*b*-TCL-based micelles displayed no toxicities to HUVECs (Figure 3A), or to 4T1 cells or HMECs (Figure 3B), at any dose level. For the positive control (20 µg/mL cisplatin), less than 2% survival was observed for all cases (data not shown).

We next examined *in vivo* toxicities to BALB/c mice following IV tail-vein injection of PBS (control), unloaded, and PZn₃-loaded PEG-*b*-TCL-based micelles (150 µL of a 5 mg/mL suspension; n = 6 animals per group). The body weights of mice were monitored daily after a single dose administration (Figure S3A), which served as a gross indicator of toxicity. At 3 and 14-days post-treatment, 3 mice from each group were randomly selected and terminal blood draws were conducted via cardiac puncture for serologic determination of renal studies (Figure S3B), liver function tests (Figure S3C), complete blood counts (Figure S3D), and white blood cell differential counts (Figure S3E). After sacrifice, organs were harvested

and fixed with formalin for H&E analysis (Figure S4). None of the mice experienced weight loss that was in excess of 10% of their initial body mass following treatment; they did not show other signs of toxicity, such as lethargy or lack of grooming; they exhibited normal serologic and hematologic results; and, there was no evidence of gross architectural distortion in any normal organ by histology. As such, both the unloaded and PZn₃-loaded PEG-*b*-TCL-based micelles were deemed safe at this dose and follow-up interval, exhibiting no signs of acute toxicities to the animals.

Novel Methods for Minimally Invasive Pharmacokinetic Analyses

BALB/c were injected with PZn₃-loaded PEG-*b*-TCL-based micelles via IV tail-vein injection (100 μ L of a 5 mg/mL suspension; n = 4 mice); and, *in vivo* imaging commenced at various intervals over a 24 h period. The results demonstrated that the micelles could be non-invasively and directly observed in the organs of the animal (Figure 4A). Small volume blood draws (15–100 μ L) were collected from the submandibular vein of each animal at analogous time points. Fluorescence measurements made of the microcapillary tubes (Figure 4B) enabled quantification of the micelle concentration in plasma, using a predetermined standard curve (Figure S5). The plots further demonstrated a marked consistency between measurements made from different mice and demonstrated that a large amount of the micelles remained in the circulation at 24 h after treatment. The average circulatory half-lives for PEG(2k)-*b*-TCL(11.2k)-based micelles was determined to be 19.6 ± 4.6 h (Table 1).

Biodistribution Studies in Nontumor-bearing Mice

Whole-animal *in vivo* fluorescence imaging was also conducted on the same mice and at the analogous time points to those described for the PK study (*vide supra*). The images revealed that the majority of the PZn₃-loaded PEG-*b*-TCL-based micelles accumulated within the liver and spleen of each animal, which are known organs for nanoparticle accumulation (10, 30). *Ex vivo* organ fluorescence measurements of excised organs made upon animal sacrifice confirmed these results (Figure 4). In addition, significant fluorescence was observed above background in all organs and was most likely due to micelles that were still present in the circulation at the time of animal sacrifice, which occurred at 24 h after micelle administration. The alfalfa in the chow likely contributed to the fluorescence signals that were observed in the gastrointestinal organs.

Tumor Accumulation in an Orthotopic Breast Cancer Model

4T1 tumors were grown in the mammary fat pads of BALB/c mice, establishing an orthotopic murine model of breast cancer. Once tumor diameters had reached at least 5 mm in diameter, the mice were treated with PZn₃-loaded PEG-*b*-TCL-based micelles via IV tail-vein injection (150 μ L of a 5 mg/mL suspension; n = 4 mice). Using *in vivo* optical imaging, the biodistribution of the micelles was observed in real time by following the emission of PZn₃ (Figure 4C and S6). The PZn₃-loaded PEG-*b*-TCL-based micelles were distributed throughout the systemic vasculature immediately upon injection, and began to accumulate at high levels in the livers and tumors of the animals (and at lower levels in their spleens) within 3.5 h of administration. By plotting the average radiant efficiency of the tumor versus time, they were found to continue to accumulate within 4T1 tumors over a period of days, peaking at ~48 h after administration (Figure 4D). The organs of each animal were collected

at the time of sacrifice and were imaged using the IVIS instrument (Figure 4E). A plot of the relative emission intensities was used to compare the final biodistribution of the micelles in each organ (Figure 4F). These *ex vivo* imaging results strongly correlated with the *in vivo* imaging data and showed that the strongest signal intensities were observed in the tumor and in the liver of each animal.

DISCUSSION

Currently available contrast agents for molecular tumor imaging are limited by their high costs, low material or signal stabilities, their poor detection sensitivities, and/or their inherent material toxicities (3, 31, 32). While optical imaging agents hold tremendous potential for the detection of superficial tumors of the breast, head & neck, or skin (33–35), and are being further developed in conjunction with endoscopic techniques to detect tumors deep in the colon and lungs (36, 37), the lack of highly sensitive and safe probes have limited their wide-spread clinical application (3). Our previous studies have established the remarkable spectroscopic properties of the NIR fluorophore PZn₃ (13, 14, 26) and have shown that it may be incorporated in biocompatible polymeric vesicles at high loading concentrations (7, 14–16, 18). We have further shown that PZn₃ generates highly sensitive fluorescent signals that enable optical imaging through deep tissue (3, 7) for both preclinical and translational clinical applications (3, 7, 17, 19, 20). In this study, we sought to develop a novel nanoparticle vehicle that was specifically designed to deliver this highly-emissive and organic-based NIR fluorophore, generating a sensitive and fully biodegradable contrast agent aimed at translational optical imaging applications.

A monodisperse suspension of polymeric micelles was generated by spontaneous self-assembly upon aqueous hydration of PEG-*b*-TCL polymer followed by gentle heating, exhibiting ideal properties for scaled-up manufacturing. The micelles allowed for facile incorporation of the high emission dipole strength porphyrin-based fluorophore PZn₃, exhibiting uniform size, marked colloidal stability, and prolonged emission in physiological environments. Previous work in our group has demonstrated that once PZn₃ is loaded in non-degradable polymeric nanoparticles, it demonstrates consistent optical properties over the course of weeks to months in aqueous suspension (7, 14, 15). The fluorophore is completely insoluble in the absence of the polymeric vehicle, exhibiting rapid aggregation and no discernable emission in aqueous solution. Nonbiodegradable PZn₃-loaded nanoparticles show no changes in particle size during that time period (by DLS), supporting that the particle architecture is stable and hence the consistent emission of PZn₃ implies the chemical stability of the particles without otherwise leakage of the fluorophore from these intact nanoparticles. As such, we have previously utilized changes in PZn₃ emission when loaded in biodegradable polymeric nanoparticles to serve as a proxy for their rate of degradation (16), which result in PZn₃ loss to the greater aqueous solution and hence quenching of its fluorescence. In this current study, while PEG-*b*-TCL-based micelles demonstrated no changes in their hydrodynamic size as assessed over 30 days in different environments (i.e. pH = 7.4 vs. pH = 5.50), they did show loss of their emission intensities. While the DLS data show that PEG-*b*-TCL micelles have consistent sizes in aqueous solution, we know from our previous experience that PZn₃ does not “leak” from intact nanoparticles but rather is only lost (and hence experiences a decay in fluorescence) due to

polymer degradation. By mapping changes in the area under the curve (AUC) for emission in plasma samples containing PZn₃-loaded PEG-*b*-TCL-based micelles, an emission half-life of ~58 h was determined; this value serves as a proxy for the rate of loss of polymer in plasma at 37 °C from otherwise structurally intact PEG-*b*-TCL-based micelles.

PZn₃-loaded PEG-*b*-TCL-based micelles demonstrated no *in vitro* or *in vivo* toxicities but generated highly sensitive optical signals that enabled detection via *in vivo* optical imaging.

The emission of PZn₃-loaded PEG-*b*-TCL-based micelles in whole blood enabled the establishment and validation of a novel method to quantify pharmacokinetics based on *ex-vivo* imaging of NIR fluorescence: we demonstrated the use of PZn₃ emission in borosilicate glass microcapillary tubes, containing blood that was collected at various time points for quantification of plasma concentration longitudinally. This novel method was minimally invasive, highly robust, and enabled accurate PK determination from small blood volumes (< 20 µL), obviating the need for repeated anesthesia and imaging, for regular tail-vein bleeding, or for the sacrifice of a multitude of mice (22).

The micelles were found to have a prolonged circulatory half-life (~20 h) and to preferentially accumulate within orthotopic tumors in a murine model of breast cancer. *In vivo* fluorescence measurements revealed that the micelles continued to accumulate within the tumor microenvironment for at least 48 h following their systemic administration, which is a time period that is substantially longer than that observed with conventional liposomal formulations and which is in contrast with the reported washout of liposomes that has been shown to occur after 24 h (38, 39). These properties make PZn₃-loaded PEG-*b*-TCL-based micelles particularly attractive for further development as optical contrast agents for *in vivo* tumor detection. Note that although the radiant efficiency can be measured quantitatively *in vivo*, this does not map directly to concentration due to confounding factors including source depth, absorption, and scattering. Thus, this approach provides a relative measure of accumulation for similarly positioned organs/tumors. In contrast, the capillary tube measurements used to quantify plasma concentrations is truly quantitative as it can be mapped back to a concentration using the calibration curve (Figure S5).

In conclusion, we demonstrate that PEG-*b*-TCL-based micelles represent a safe and fully biodegradable nanoscale delivery vehicle with ideal characteristics for tumor imaging and theranostic development. The incorporation of the highly emissive tris(porphyrin)-based NIR fluorophore PZn₃ into the micelles introduced a novel optical contrast agent that was fully biodegradable and that possessed the requisite sensitivity for deep tissue imaging. In order to study the preclinical pharmacology of PZn₃-loaded PEG-*b*-TCL-based micelles, we improved upon conventional methods for non-invasive imaging to demonstrate direct visualization of *in vivo* circulation and nanoparticle biodistribution. We further developed a novel optical imaging technique that enabled minimally invasive pharmacokinetics analyses, using minute quantities of blood that were directly imaged in microcapillary tubes. The superior biomaterial properties of PZn₃-loaded PEG-*b*-TCL-based micelles support their further development for translational cancer imaging and/or drug delivery applications.

Supplementary Material

Refer to Web version on PubMed Central for supplementary material.

Acknowledgments

Funding was provided from a training grant (5T32GM008555-18; awarded to MWD) and an SBIR grant from the National Institutes of Health (1R43CA159527-01A1; awarded to Vindico NanoBioTechnology, Inc.). PPG acknowledges research support from the Charles W. and Jennifer C. Johnson Clinical Investigator fund and from the Kathryn Fox Samway Foundation. MJT acknowledges funding from the Department of Defense (W81XWH-13-1-0086). The authors would also like to thank the Controlled Release Society for awarding this work with the CRS Outstanding Preclinical Sciences & Animal Health Best Paper Award at the 2013 annual meeting in Honolulu, HI. The authors also acknowledge use of the Optical Molecular Imaging and Analysis shared resource, which is supported by the Duke Cancer Institute. The authors would like to acknowledge Taylor Gill for her assistance in preparing the micelles used in these studies and Dr. Jennifer Ayres for her help with fluorescence spectroscopy. The authors are grateful to Dr. Kathleen Ashcraft for her advice on cell studies and for her assistance with tumor injections.

References

- Hong G, Antaris AL, Dai H. Near-infrared fluorophores for biomedical imaging. *Nature Biomedical Engineering*. Jan 10.2017 2017:1.
- Zhang RR, Schroeder AB, Grudzinski JJ, Rosenthal EL, Warram JM, Pinchuk AN, et al. Beyond the margins: real-time detection of cancer using targeted fluorophores. *Nat Rev Clin Oncol*. 2017 Jan 17.
- Ghoroghchian PP, Therien MJ, Hammer DA. In vivo fluorescence imaging: a personal perspective. *WIREs Nanomed Nanobiotechnol*. 2009; 1(2):156–67.
- Whitley MJ, Cardona DM, Lazarides AL, Spasojevic I, Ferrer JM, Cahill J, et al. A mouse-human phase 1 co-clinical trial of a protease-activated fluorescent probe for imaging cancer. *Sci Transl Med*. 2016 Jan 06.8(320):320ra4.
- Kuchimaru T, Iwano S, Kiyama M, Mitsumata S, Kadonosono T, Niwa H, et al. A luciferin analogue generating near-infrared bioluminescence achieves highly sensitive deep-tissue imaging. *Nat Commun*. 2016 Jun 14.7:11856. [PubMed: 27297211]
- Deng H, Zhong Y, Du M, Liu Q, Fan Z, Dai F, et al. Theranostic self-assembly structure of gold nanoparticles for NIR photothermal therapy and X-Ray computed tomography imaging. *Theranostics*. 2014; 4(9):904–18. [PubMed: 25057315]
- Ghoroghchian PP, Frail PR, Susumu K, Blessington D, Brannan AK, Bates FS, et al. Near-infrared-emissive polymersomes: self-assembled soft matter for in vivo optical imaging. *Proc Natl Acad Sci U S A*. 2005 Feb 22; 102(8):2922–7. [PubMed: 15708979]
- Qi W, Ghoroghchian PP, Li G, Hammer DA, Therien MJ. Aqueous self-assembly of poly(ethylene oxide)-block-poly(epsilon-caprolactone) (PEO-b-PCL) copolymers: disparate diblock copolymer compositions give rise to nano- and meso-scale bilayered vesicles. *Nanoscale*. 2013 Nov 21; 5(22):10908–15. [PubMed: 24056924]
- Ghoroghchian PP, Li G, Levine DH, Davis KP, Bates FS, Hammer DA, et al. Bioresorbable vesicles formed through spontaneous self-assembly of amphiphilic poly(ethylene oxide)-block-polyepsilon-caprolactone. *Macromolecules*. 2006 Mar 7; 39(5):1673–5. Epub 2006/03/07. Eng. [PubMed: 20975926]
- Moghimi SM, Hunter AC, Murray JC. Long-circulating and target-specific nanoparticles: theory to practice. *Pharmacol Rev*. 2001 Jun; 53(2):283–318. [PubMed: 11356986]
- Matsumura Y, Maeda H. A new concept for macromolecular therapeutics in cancer chemotherapy: mechanism of tumoritropic accumulation of proteins and the antitumor agent smancs. *Cancer research*. 1986 Dec; 46(12 Pt 1):6387–92. [PubMed: 2946403]
- Chapanian R, Tse MY, Pang SC, Amsden BG. The role of oxidation and enzymatic hydrolysis on the in vivo degradation of trimethylene carbonate based photocrosslinkable elastomers. *Biomaterials*. 2009 Jan; 30(3):295–306. Epub 2008/10/25. eng. [PubMed: 18947866]

13. Duncan TV, Susumu K, Sinks LE, Therien MJ. Exceptional near-infrared fluorescence quantum yields and excited-state absorptivity of highly conjugated porphyrin arrays. *J Am Chem Soc.* 2006 Jul 19; 128(28):9000–1. Epub 2006/07/13. eng. [PubMed: 16834350]
14. Duncan TV, Ghoroghchian PP, Rubtsov IV, Hammer DA, Therien MJ. Ultrafast Excited-State Dynamics of Nanoscale Near-Infrared Emissive Polymersomes. *Journal of the American Chemical Society* 2008. 2008 Jul 01; 130(30):9773–84.
15. Ghoroghchian PP, Lin JJ, Brannan AK, Frail PR, Bates FS, Therien MJ, et al. Quantitative membrane loading of polymer vesicles. *Soft Matter.* 2006 Nov 7; 2(11):973–80.
16. Ghoroghchian PP, Frail PR, Li G, Zupancich JA, Bates FS, Hammer DA, et al. Controlling bulk optical properties of emissive polymersomes through intramembranous polymer-fluorophore interactions. *Chem Mater.* 2007 Mar 20; 19(6):1309–18. Epub 2007/03/20. Eng. [PubMed: 19079789]
17. Levine DH, Ghoroghchian PP, Freudenberg J, Zhang G, Therien MJ, Greene MI, et al. Polymersomes: a new multi-functional tool for cancer diagnosis and therapy. *Methods (San Diego, Calif).* 2008; 46(1):25–32.
18. Ghoroghchian PP, Frail PR, Susumu K, Park TH, Wu SP, Uyeda HT, et al. Broad spectral domain fluorescence wavelength modulation of visible and near-infrared emissive polymersomes. *J Am Chem Soc.* 2005 Nov 9; 127(44):15388–90. Epub 2005/11/03. eng. [PubMed: 16262400]
19. Wu SP, Lee I, Ghoroghchian PP, Frail PR, Zheng G, Glickson JD, et al. Near-infrared optical imaging of B16 melanoma cells via low-density lipoprotein-mediated uptake and delivery of high emission dipole strength tris[(porphinato)zinc(II)] fluorophores. *Bioconjugate Chemistry.* 2005; 16(3):542–50. [PubMed: 15898720]
20. Christian NA, Milone MC, Ranka SS, Li G, Frail PR, Davis KP, et al. Tat-functionalized near-infrared emissive polymersomes for dendritic cell labeling. *Bioconjugate Chemistry.* 2007; 18(1): 31–40. [PubMed: 17226955]
21. Katz JS, Eisenbrown KA, Johnston ED, Kamat NP, Rawson J, Therien MJ, et al. Soft biodegradable polymersomes from caprolactone-derived polymers. *Soft Matter.* 2012; 8(42): 10853–62.
22. Kurawattimath V, Pocha K, Thanga Mariappan T, Trivedi R, Mandlekar S. A modified serial blood sampling technique and utility of dried-blood spot technique in estimation of blood concentration: application in mouse pharmacokinetics. *Eur J Drug Metab Pharmacokinet* 2012. 2012 Mar 01; 37(1):23–30.
23. Kunjachan S, Detappe A, Kumar R, Ireland T, Cameron L, Biancur DE, et al. Nanoparticle Mediated Tumor Vascular Disruption: A Novel Strategy in Radiation Therapy. *Nano letters.* 2015 Nov 11; 15(11):7488–96. [PubMed: 26418302]
24. Detappe A, Kunjachan S, Sancey L, Motto-Ros V, Biancur D, Drane P, et al. Advanced multimodal nanoparticles delay tumor progression with clinical radiation therapy. *Journal of controlled release: official journal of the Controlled Release Society.* 2016 Sep 28.238:103–13. [PubMed: 27423325]
25. Detappe A, Thomas E, Tibbitt MW, Kunjachan S, Zavidij O, Parnandi N, et al. Ultrasmall Silica-Based Bismuth Gadolinium Nanoparticles for Dual Magnetic Resonance-Computed Tomography Image Guided Radiation Therapy. *Nano Lett.* 2017 Feb 02.
26. Susumu K, Therien MJ. Decoupling optical and potentiometric band gaps in π -conjugated materials. *J Am Chem Soc.* 2002 Jul 24; 124(29):8550–2. Epub 2002/07/18. eng. [PubMed: 12121095]
27. Corporation C. Living Image(R) Software User's Manual Version 42. Hopkinton, MA: Caliper Life Sciences; 2011. ROI Tools.
28. Cao Y, Li CY, Moeller BJ, Yu D, Zhao Y, Dreher MR, et al. Observation of incipient tumor angiogenesis that is independent of hypoxia and hypoxia inducible factor-1 activation. *Cancer research.* 2005 Jul 1; 65(13):5498–505. Epub 2005/07/05. eng. [PubMed: 15994919]
29. Elsabahy M, Heo GS, Lim SM, Sun G, Wooley KL. Polymeric Nanostructures for Imaging and Therapy. *Chemical reviews.* 2015 Oct 14; 115(19):10967–1011. [PubMed: 26463640]
30. Chauhan VP, Martin JD, Liu H, Lacorre DA, Jain SR, Kozin SV, et al. Angiotensin inhibition enhances drug delivery and potentiates chemotherapy by decompressing tumour blood vessels. *Nat Commun.* 2013; 4:2516. [PubMed: 24084631]

31. Alford R, Simpson HM, Duberman J, Hill GC, Ogawa M, Regino C, et al. Toxicity of Organic Fluorophores Used in Molecular Imaging: Literature Review. *Mol Imaging*. 2009 Nov-Dec;8(6): 341–54. [PubMed: 20003892]
32. Kobayashi H, Ogawa M, Alford R, Choyke PL, Urano Y. New strategies for fluorescent probe design in medical diagnostic imaging. *Chem Rev*. 2010 May 12; 110(5):2620–40. [PubMed: 20000749]
33. Ntziachristos V. Going deeper than microscopy: the optical imaging frontier in biology. *Nat Methods*. 2010 Aug; 7(8):603–14. [PubMed: 20676081]
34. Keereweer S, Sterenborg HJCM, Kerrebijn JDF, Van Driel PBAA, de Jong RJB, Lowik CWGM. Image-Guided Surgery in Head and Neck Cancer: Current Practice and Future Directions of Optical Imaging. *Head Neck-J Sci Spec*. 2012 Jan; 34(1):120–6.
35. Burrows PE, Gonzalez-Garay ML, Rasmussen JC, Aldrich MB, Guilliod R, Maus EA, et al. Lymphatic abnormalities are associated with RASA1 gene mutations in mouse and man. *P Natl Acad Sci USA*. 2013 May 21; 110(21):8621–6.
36. Gioux S, Choi HS, Frangioni JV. Image-guided surgery using invisible near-infrared light: fundamentals of clinical translation. *Molecular imaging*. 2010 Oct; 9(5):237–55. [PubMed: 20868625]
37. Becker A, Hassenius C, Licha K, Ebert B, Sukowski U, Semmler W, et al. Receptor-targeted optical imaging of tumors with near-infrared fluorescent ligands. *Nature biotechnology*. 2001 Apr; 19(4):327–31.
38. Charrois GJ, Allen TM. Rate of biodistribution of STEALTH liposomes to tumor and skin: influence of liposome diameter and implications for toxicity and therapeutic activity. *Biochim Biophys Acta*. 2003 Jan 10; 1609(1):102–8. Epub 2003/01/01. eng. [PubMed: 12507764]
39. Gabizon AA. Selective tumor localization and improved therapeutic index of anthracyclines encapsulated in long-circulating liposomes. *Cancer Research*. 1992 Feb 15; 52(4):891–6. [PubMed: 1737351]

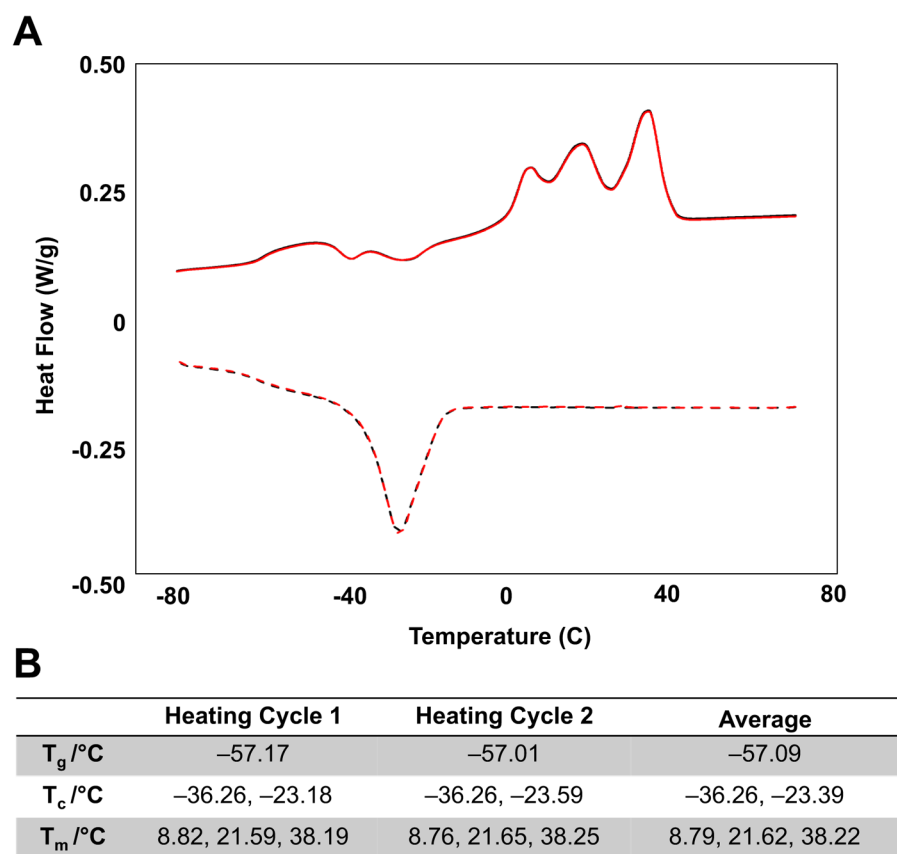


Figure 1. Differential scanning calorimetry of the PEG(2k)-*b*-TCL(11.2k) copolymer
 The sample was heated between -80 and $+80^\circ\text{C}$ at $5^\circ\text{C}/\text{min}$ ramp. (A) Plot of its phase transitions as a function of temperature. (B) Table of major transitions seen in repeated heating cycles. T_g : glass transition temperature, T_c : crystallization temperature, T_m : melting temperature.

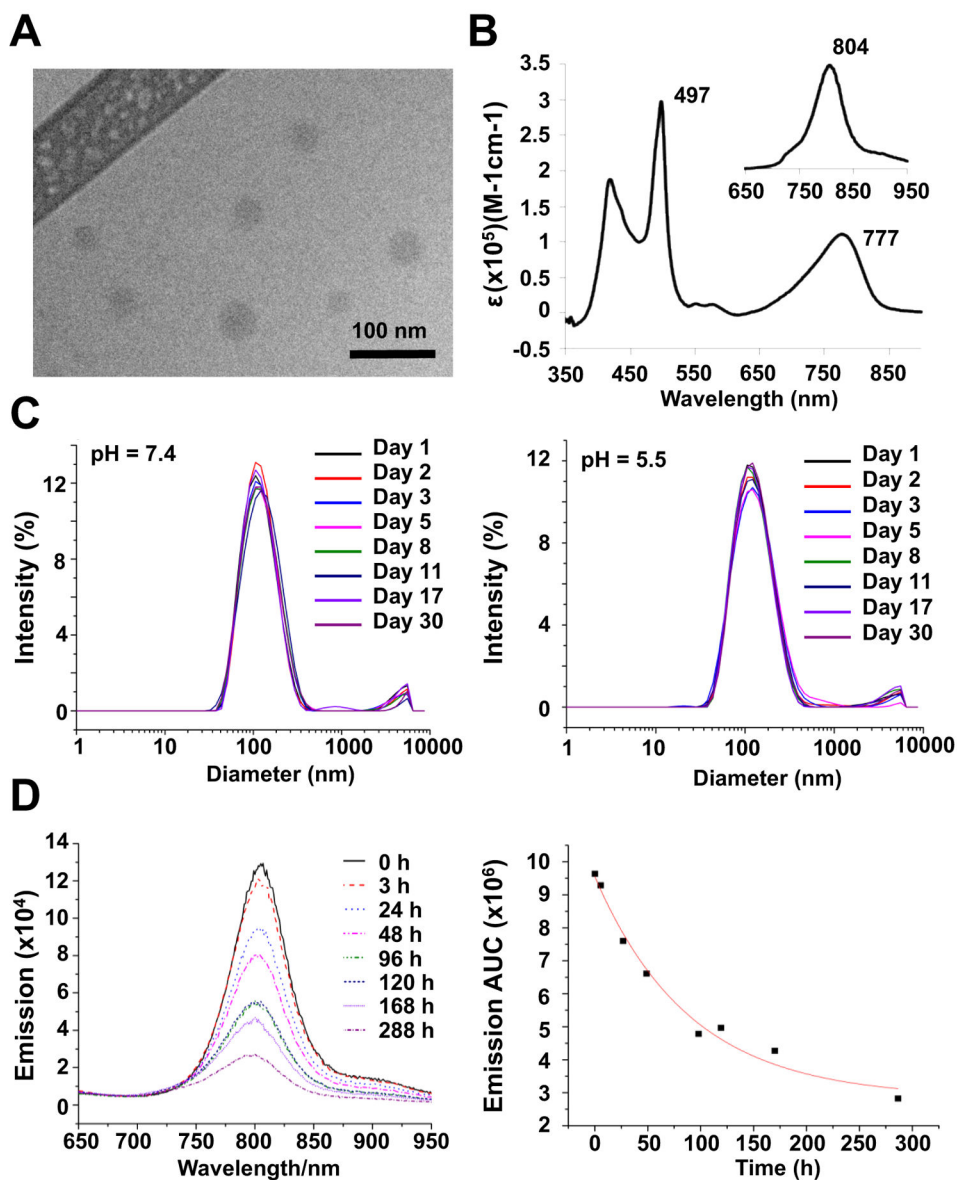


Figure 2. *In situ* Stability of the PZN₃-loaded PEG-*b*-TCL-based micelles

(A) Cryo-TEM image, (B) absorbance spectrum that is corrected for light scattering, and (inset) fluorescence emission spectrum of PZN₃-loaded PEG-*b*-TCL-based micelles in aqueous suspension ($\lambda_{\text{ex}} = 492 \text{ nm}$). (C) Changes in the hydrodynamic size over 30 days in different environments (pH = 7.4 vs. pH = 5.50). (D) Variation of the emission intensities of PZN₃ in aqueous suspensions of PEG-*b*-TCL-based micelles that were placed in plasma at 37 °C and as a function of time. Integration of the emissive signal from PZN₃ over time (right) was obtained by calculating the area under the curve (AUC) and was used to determine its fluorescence emission half-life within micelles suspensions upon transfer to plasma. ϵ : extinction coefficient.

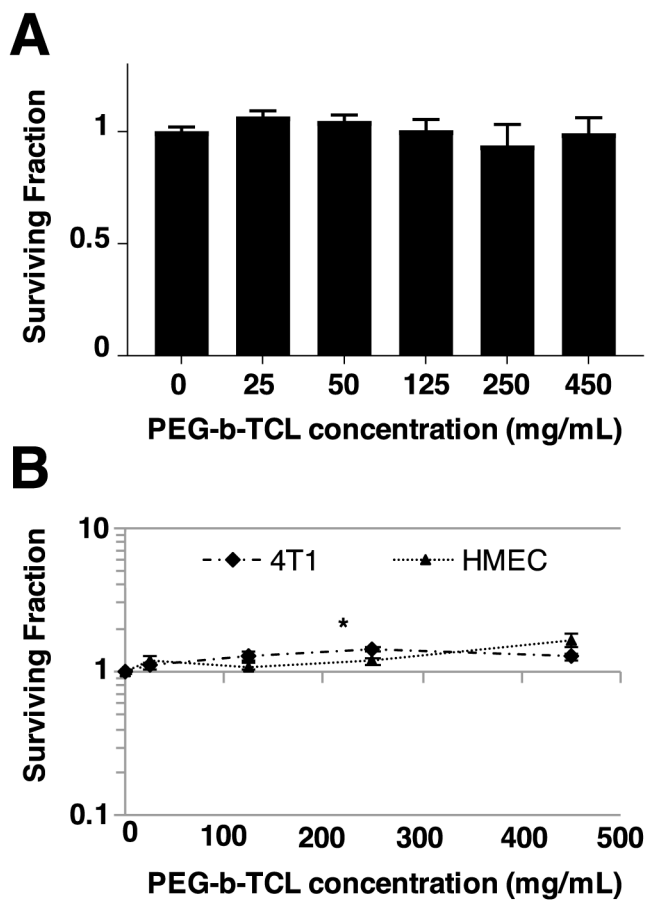


Figure 3. *In vitro* and *In vivo* Toxicity of PEG-*b*-TCL-based Micelles

Cellular viability assays on established cells lines demonstrating minimal toxicity of PZn₃-loaded PEG-*b*-TCL-based micelles to (A) HUVECs (CellGlo-Titer assay), (B) 4T1, and HMECs (clonogenics assays). For the clonogenics assays, 4T1 and HEMCs were treated with micelles for 24 h, plated at low density, and allowed to grow for 4–10 days. The numbers of colonies were then counted and compared to the numbers obtained from untreated (control) cells. Data presented as mean ± SD. 4T1: mouse mammary carcinoma cells, HMEC: human mammary epithelial cells, * $p < 0.05$, unpaired, 2-sided t-test compared to PBS control.

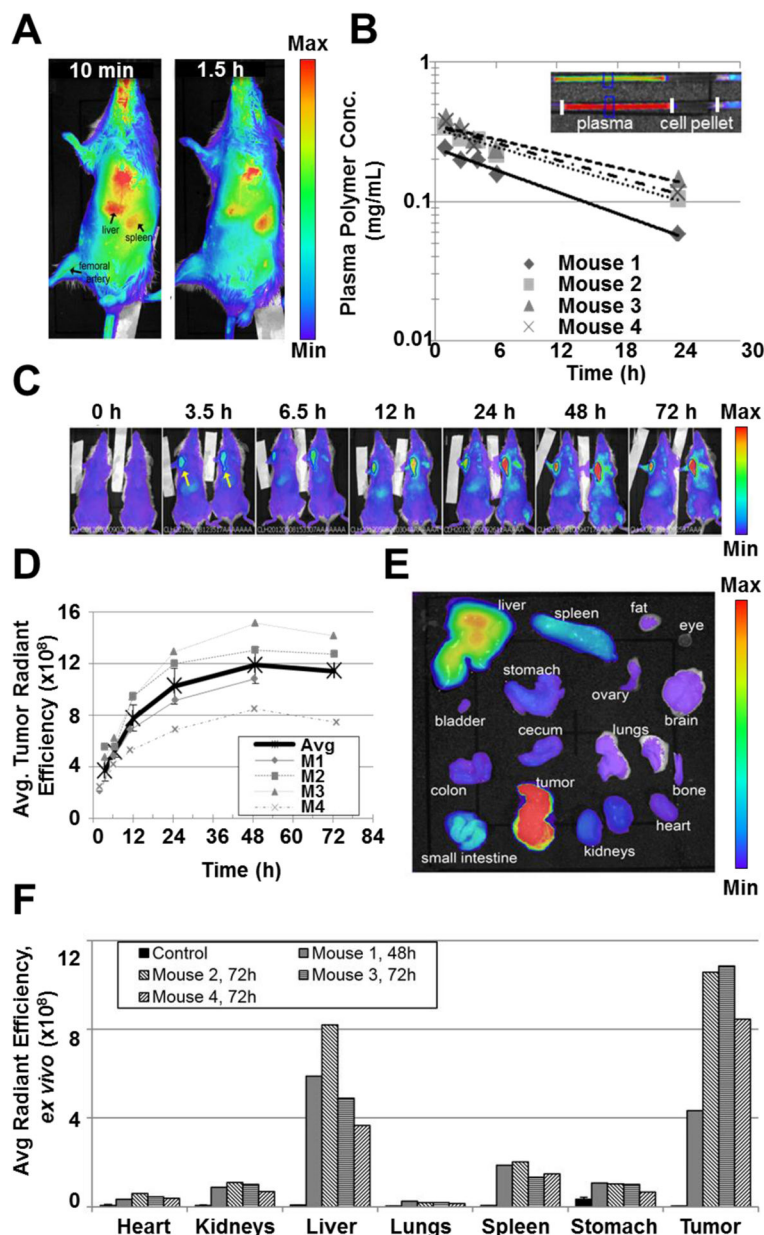


Figure 4. Pharmacokinetics and *in vivo* tumor accumulation of PZn₃-loaded PEG-*b*-TCL-based micelles

(A) Whole-animal optical imaging was performed, gating on PZn₃ emissive signals from micelles at various time points after systemic administration via IV tail-vein injection. (B) Change in plasma concentration over time for each mouse after treatment with PZn₃-loaded PEG-*b*-TCL-based micelles, as measured by the fluorescence of plasma samples using the IVIS[®] Kinetic Imaging instrument ($\lambda_{\text{ex}} = 745 \text{ nm}$, $\lambda_{\text{em}} = 810\text{--}875 \text{ nm}$). (C) Representative overlay of photographic and fluorescence images of 4T1 tumor-bearing mice at various time points after IV tail-vein administration of a suspension of 60 nm diameter PZn₃-loaded PEG-*b*-TCL-based micelles. Whole body imaging was conducted with the IVIS[®] Kinetic Imaging instrument ($\lambda_{\text{ex}} = 745 \text{ nm}$, $\lambda_{\text{em}} = 810\text{--}875 \text{ nm}$), exhibiting accumulation of the

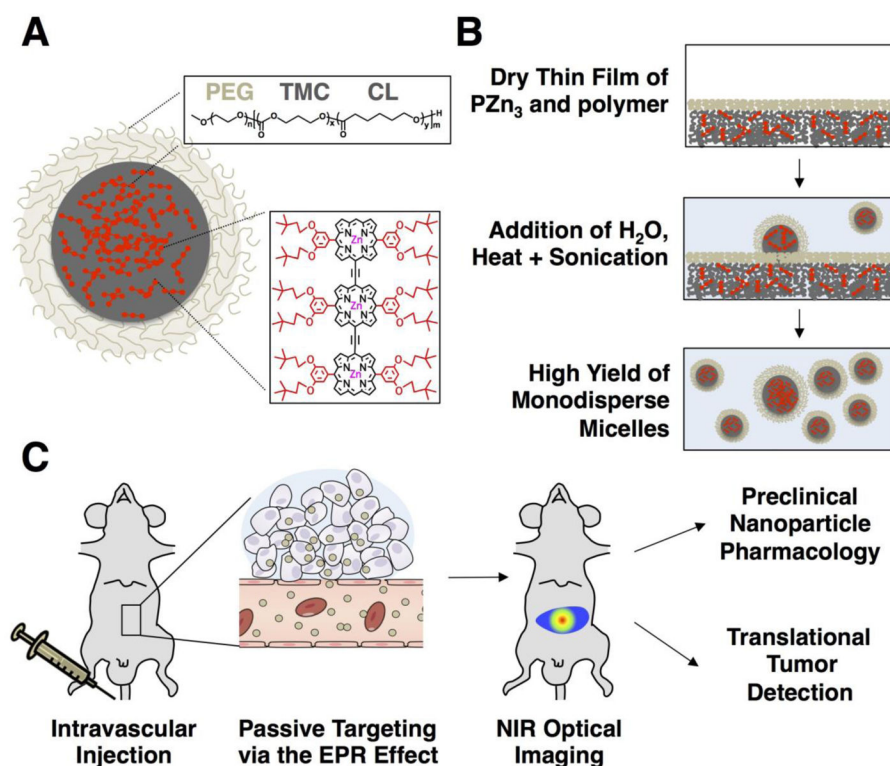
micelles within the orthotopic 4T1 tumors implanted in the mammary fat pads (arrows), livers, and spleens of the animals (n = 2 of a total of 4 treated animal displayed at each time point). (D) Changes in the average radiant efficiencies of tumors over time following treatment with PZn₃-loaded PEG-*b*-TCL-based micelles, as measured via *in vivo* optical imaging. Thick black line represents the average, error bars \pm SEM. (E) Representative fluorescence image of excised organs at 48 h after treatment. (F) *Ex vivo* fluorescence quantification of organs from tumor-bearing mice harvested at 48 or 72 h after IV tail-vein injection of PZn₃-loaded PEG-*b*-TCL-based micelles.

Author Manuscript

Author Manuscript

Author Manuscript

Author Manuscript



Scheme 1. Near-infrared Emissive PEG-*b*-TCL-based Micelles

(A) Chemical structure of micelles formed from the PEG-*b*-TCL copolymer and the high-emission dipole strength, tris(porphyrin)-based fluorophore PZn₃. (B) Schematic representation of the formation of PZn₃-loaded PEG-*b*-TCL-based micelles under gentle fabrication conditions. (C) Schematic representation of the administration of the PZn₃-loaded PEG-*b*-TCL-based micelles into mice via intravenous tail-vein injection, their uptake into tumors by passive targeting, and the applications of these agents. PEG: poly(ethylene-glycol), TMC: trimethylene carbonate block, CL: caprolactone block, PZn₃: ethynyl-bridged tris(porphinato)zinc-based NIR fluorophore.

Table 1

Results of PK curve fitting for mice that were administered PZn₃-loaded PEG-*b*-TCL-based micelles via IV tail-vein injection. $C=C_0 \exp(-kt)$

Mouse	C_0 (mg/mL)	k (days ⁻¹)	R^2	Half-lives (h)	AUC (mg*h/mL)	Mean Residence Time (hr)
1	0.24	1.16	0.99	14.4	2.90	16.4
2	0.33	0.89	0.98	18.7	4.34	21.5
3	0.35	0.65	0.87	25.5	4.86	33.8
4	0.35	0.84	0.96	19.7	4.54	22.8
Average	0.32	0.89	0.924	19.6	4.16	23.6
St Dev	±0.05	±0.21	±0.027	±4.6	±0.87	±7.3

The elimination half-lives were determined for each mouse based on the data fit from Fig. 4: $t_{1/2} = \ln(2)/k$. Areas under the curve (AUCs) and mean residence time were calculated using a non-compartmental model with the AUC and NCA functions from the PK library in R.